Sound generation in the hole-tone feedback problem (Mathematical Physics and Application of Nonlinear Wave Phenomena)

AUTHOR(S):

Langthjem, Mikael A.; Nakano, Masami

CITATION:

Langthjem, Mikael A. ...[et al]. Sound generation in the hole-tone feedback problem (Mathematical Physics and Application of Nonlinear Wave Phenomena). 数理解析研究所講究録 2009, 1645: 221-230

ISSUE DATE:

2009-04

URL:

http://hdl.handle.net/2433/140660

数理解析研究所講究録
第1645巻 2009年 221-230

Sound generation in the hole-tone feedback problem

Mikael A. Langthjem† and Masami Nakano‡

†*Graduate School of Science and Technology, Yamagata University, Jonan 4-chome, Yonezawa-shi, 992-8510 Japan*

‡*Institute of Fluid Science, Tohoku University, 2-1-1 Katahira, Aoba-ku, Sendai-shi, 980-8577 Japan*

Abstract

The paper describes a numerical method for aeroacoustic analysis of an axisymmetric problem of self-sustained flow oscillations (the hole-tone problem). The method is based on the Powell-Howe theory of vortex sound and the special boundary element method for thin bodies, developed by Terai. A specific case is analyzed and compared with experiments; reasonably good agreement is found.

Keywords: self-sustained flow oscillations; axisymmetric vortex method; vortex sound; boundary element method

1 Introduction

The present work is concerned with computation of the sound generated by self-sustained flow oscillations in the so-called hole-tone problem. Here a jet issued from a circular nozzle impinges upon a similar hole in a thin plate fixed a little downstream from the nozzle. The problem is described in Lord Rayleigh's *Theory of Sound* (1945)[1], § 371; it is also considered in Howe (1998). Comprehensive reviews, covering also related problems, have been given by Rockwell and Naudascher (1979) and Rockwell (1983).

A number of experimental studies on the hole tone problem have been published (Chanaud and Powell 1965, Nakano *et al.* 2004). Theoretical and numerical studies are however few. The authors have previously carried out a numerical study of the problem, based on an axisymmetric discrete vortex method and an aeroacoustic model based on Curle's equation (Howe 1998). The problem is however one of 'pure' vortex sound, and the theory developed by Powell (1964) and Howe (1975) is the proper one to use.

The aim of the present work is thus to develop a numerical method for the hole-tone problem, based on the theory of vortex sound, in an axisymmetric setting[2]. The experimental measurements, to which the numerical results are to be compared, are carried out not too far away from the jet, within the outer edge of the end plate. In order to take the scattering of the end plate properly into account, a special boundary element method for thin bodies, developed by Terai (1980), is employed, rather than often applied compact Green's function method.

[1]Originally published 1877 (1. ed.) and 1894 (2. ed.).

[2]Rayleigh (1945) pointed out that the disturbances remain axisymmetric. This was also the conclusion of Chanaud and Powell (1965).

2 Modeling of the basic jet flow

An axisymmetric jet of radius $r = r_0$ is discharging from a nozzle at $x = 0$ in the axisymmetric cylindrical polar coordinate system (x, r); see Fig. 1. The shear layer of the jet is impinging upon the edge of a circular hole, also of radius r_0, in a parallel end plate, placed at $x = \ell$. The

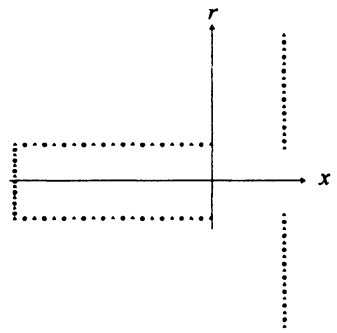

Figure 1: Axisymmetric cylindrical polar coordinates used to describe the basic jet flow. A cut through the nozzle (with mean-flow-generating vortices on the back) and the end plate is also shown.

shear layers of the jets issued from the nozzle and from the end plate are thought to be first represented by continuous vortex sheets. The nozzle and the end plate are represented by bound vortex sheets. These vortex sheets are then discritized into necklaces of discrete vortex rings.

Vortex ring theory

The vortex ring model of Nitsche and Krasny (1994) is used. This is a 'desingularized' version of the thin-cored circular vortex ring described in, e.g., Lamb's *Hydrodynamics* (1993). The induced velocity $\mathbf{u} = (u_x, u_r)$ at a location (x, r), from a single vortex ring of strength Γ and located at (x_i, r_i), is obtained from

$$u_x = \frac{1}{r}\frac{\partial \Psi}{\partial r}\,, \quad u_r = -\frac{1}{r}\frac{\partial \Psi}{\partial x}, \tag{1}$$

where the stream function Ψ is given by

$$\begin{aligned} \Psi(x, r, x_i, r_i) &= \frac{\Gamma}{2\pi}(\eta_1 + \eta_2)\left\{K(\lambda) - E(\lambda)\right\}, \\ \lambda &= (\eta_2 - \eta_1)/(\eta_2 + \eta_1), \\ \eta_1 &= \left\{(x - x_i)^2 + (r - r_i)^2 + \epsilon^2\right\}^{\frac{1}{2}}, \\ \eta_2 &= \left\{(x - x_i)^2 + (r + r_i)^2 + \epsilon^2\right\}^{\frac{1}{2}}. \end{aligned} \tag{2}$$

Here $K(\lambda)$ and $E(\lambda)$ are the complete elliptic integrals of first and second kind, respectively (Abramowitz and Stegun 1972). The parameter ϵ in the η_1 and η_2 functions is a smoothing, or regularization, parameter, corresponding in effect to a finite vortex sheet thickness. It may also be thought of as 'artificial' viscosity; artificial in the sense that it does not bring about any dissipation of energy.

We are not aware of any studies dealing with a theoretical determination of ϵ. Comprehensive studies have been carried out to determine numerically the 'optimum' value (Langthjem and Nakano 2005).

Modeling of solid surfaces

As mentioned above, the jet nozzle and the end plate are represented by bound vortex rings. The inviscid boundary condition of zero normal velocity is imposed at control points between these rings. The mean jet flow is also provided by a number of vortex rings placed on the 'back' of the nozzle tube. The strengths of the bound vortex rings are dictated by the boundary condition and by the mean jet velocity.

Modeling of vortex shedding

A vortex ring is released from the nozzle at each time step in the simulation. The strength of this ring is dictated by the Kutta condition, which demands that the pressure a little above the nozzle edge equals the pressure a little below. Once released, the vortex rings keep their strengths throughout the simulation. The convection velocity of a shed vortex ring is dictated by the induced velocities from all other vortex rings, plus the self-induced velocity.

3 Aeroacoustic model

The equation of vortex sound and its formal solution in terms of integral equations

For evaluating the sound generated by the self-sustained flow oscillations, the start point is taken in Howe's equation for vortex sound at low Mach numbers (Howe 2003). Let $\boldsymbol{\omega} = \nabla \times \mathbf{u}$ denote the vorticity. The sound pressure $p(\mathbf{x}, t)$ is related to the vortex force $\boldsymbol{\mathfrak{L}}(\mathbf{x}, t) = \boldsymbol{\omega}(\mathbf{x}, t) \times \mathbf{u}(\mathbf{x}, t)$ via the non-homogeneous wave equation

$$\left(\frac{1}{c_0^2}\frac{\partial^2}{\partial t^2} - \nabla^2\right) p = \rho \nabla \cdot \boldsymbol{\mathfrak{L}}. \tag{3}$$

The boundary conditions are

$$\frac{\partial p}{\partial n} = 0 \text{ on the end plate}, \quad p \to 0 \text{ for } |\mathbf{x}| \to \infty, \tag{4}$$

where n denotes the normal vector.

We define Fourier transform with respect to time t and frequency ν as

$$P(\mathbf{x}, \nu) = \frac{1}{2\pi}\int_{-\infty}^{\infty} p(\mathbf{x}, t) \mathrm{e}^{\mathrm{i}\nu t} dt, \tag{5}$$

$$p(\mathbf{x}, t) = \int_{-\infty}^{\infty} P(\mathbf{x}, \nu) \mathrm{e}^{-\mathrm{i}\nu t} d\nu. \tag{6}$$

Applying (5) to (3) gives

$$\left(\nabla^2 + k^2\right) P = -\rho \nabla \cdot \mathbf{L} \tag{7}$$

where $\mathbf{L}(\mathbf{x}, \nu)$ is the Fourier transform of $\boldsymbol{\mathfrak{L}}(\mathbf{x}, t)$, and $k = \nu / c_0$ is the wave number. To solve (7) use is made of the free-space Green's function $G(\mathbf{x}, \mathbf{y}; \nu)$ which is a solution of the equation

$$\left(\nabla^2 + k^2\right) G = -\delta(\mathbf{x} - \mathbf{y}), \tag{8}$$

where $\delta(\mathbf{x} - \mathbf{y})$ is Dirac's delta function. Here and in the sequel, $\mathbf{x}$ denotes the location of an observation point and $\mathbf{y}$ the location of an acoustic source. Finally it is noted that G satisfies the second of the boundary conditions (4).

Multiplying (7) by G and (8) by P gives, after integration and use of Green's second identity,

$$\begin{aligned} \varsigma P(\mathbf{x}, \nu) &= \rho \iiint G(\mathbf{x}, \mathbf{y}) \nabla_{\mathbf{y}} \cdot \mathbf{L}(\mathbf{y}, \nu) \, d^3\mathbf{y} \\ &- \iint \left[G(\mathbf{x}, \mathbf{y}_\beta) \frac{\partial}{\partial n_\beta} P(\mathbf{y}_\beta, \nu) - P(\mathbf{y}_\beta, \nu) \frac{\partial}{\partial n_\beta} G(\mathbf{x}, \mathbf{y}_\beta) \right] d^2\mathbf{y}_\beta. \end{aligned} \tag{9}$$

The subscript $\mathbf{y}$ on the del-operator in the first term on the right hand side indicates differentiation with respect to the source coordinates $\mathbf{y}$. The subscript β on $\mathbf{y}_\beta$ indicates a point on the end plate and n_β the normal vector at that point. The notation $d^3\mathbf{y}$ is used for $dy_1 dy_2 dy_3$ and $d^2\mathbf{y}_\beta$ for $dy_{\beta 1} dy_{\beta 2}$. The parameter ς is given by

$$\varsigma = \begin{cases} 1 & \text{when } \mathbf{x} \text{ is in the acoustic medium,} \\ \frac{1}{2} & \text{when } \mathbf{x} \text{ is on a solid boundary,} \\ 0 & \text{when } \mathbf{x} \text{ is outside the acoustic medium.} \end{cases} \tag{10}$$

Proofs of these results can be found in Petrovsky (1991).

The first of the equations (4) gives that $\partial P/\partial n_\beta = 0$. Thus the right hand side of (9) includes only two terms. The first term can, via integration by parts, be rewritten as

$$-\iiint \nabla_{\mathbf{y}} G \cdot \mathbf{L}\, d^3\mathbf{y} = -\sum_j \iiint \frac{\partial G}{\partial y_j} L_j \, d^3\mathbf{y}. \tag{11}$$

Considering a plate of vanishing thickness, Terai (1980) has shown that the pressure at a point $\mathbf{x}$ away from the plate can be expressed as

$$P(\mathbf{x}, \nu) = -\rho \sum_j \iiint \frac{\partial G(\mathbf{x}, \mathbf{y})}{\partial y_j} L_j(\mathbf{y}, \nu)\, d^3\mathbf{y} + \iint \tilde{P}(\mathbf{y}_\beta, \nu) \frac{\partial G(\mathbf{x}, \mathbf{y}_\beta)}{\partial n_\beta} d^2\mathbf{y}_\beta, \tag{12}$$

where $\tilde{P}(\mathbf{y}_\beta, \nu)$ is the pressure difference across the plate. To determine this quantity, use will be made of the normal derivative of (12) at a point $\mathbf{x}_\alpha$ on the end plate. Since $\partial P(\mathbf{x}_\alpha, \nu)/\partial n_\alpha = 0$ we obtain

$$\iint \tilde{P}(\mathbf{y}_\beta) \frac{\partial^2 G(\mathbf{x}_\alpha, \mathbf{y}_\beta)}{\partial n_\alpha \partial n_\beta} d^2\mathbf{y}_\beta = \rho \sum_i \sum_j \iiint \frac{\partial^2 G(\mathbf{x}_\alpha, \mathbf{y})}{\partial x_i \partial y_j} n_{\alpha i} L_j(\mathbf{y}, \nu)\, d^3\mathbf{y}. \tag{13}$$

This is a Fredholm integral equation of the first kind for determining the unknown pressure difference $\tilde{P}$.

The Green's function in spherical coordinates

For the specific solution of (9), (13) spherical coordinates will be employed (rather than cylindrical coordinates). Let $\mathbf{x} = (r, \theta, \phi)$ and $\mathbf{y} = (r_*, \theta_*, \phi_*)$. In the present axisymmetric case the polar axis $\theta = 0$ is the axis of symmetry. The azimuthal angle ϕ is eliminated by integration over this parameter ($0 \le \phi \le 2\pi$). Following this, the problem is expressed in terms of (r, θ), as defined in Fig. 2. The Green's function expressed in these coordinates, $G(r, \theta; \nu)$, is the solution

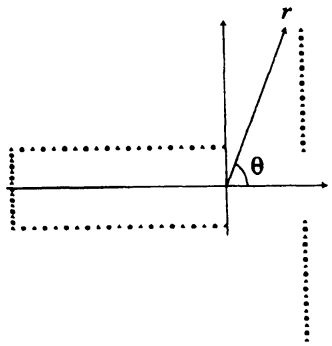

Figure 2: Axisymmetric spherical coordinates used in the acoustic analysis.

of the equation

$$\frac{1}{r^2}\frac{\partial}{\partial r}\left(r^2\frac{\partial G}{\partial r}\right)+\frac{1}{r^2\sin\theta}\frac{\partial}{\partial\theta}\left(\sin\theta\frac{\partial G}{\partial\theta}\right)+k^2G=-\frac{\delta(r-r_*)\delta(\theta-\theta_*)}{r^2\sin\theta}. \tag{14}$$

Consider first the homogeneous form of (14). Assuming a product solution on the form

$$G(r,\theta)=R(r)\Theta(\theta) \tag{15}$$

we obtain the separated equations

$$\frac{1}{r^2}\frac{d}{dr}\left(r^2\frac{dR}{dr}\right)+\left(k^2-\frac{n(n+1)}{r^2}\right)R=0, \tag{16}$$

$$\frac{1}{\sin\theta}\frac{d}{d\theta}\left(\sin\theta\frac{d\Theta}{d\theta}\right)+n(n+1)\Theta=0. \tag{17}$$

The complete solution to (16) is

$$R(r)=B_1j_n(kr)+B_2y_n(kr), \tag{18}$$

where B_1 and B_2 are constants, and $j_n(z)$ and $y_n(z)$ are the spherical Bessel functions of first and second kind, respectively, both of degree n. These functions are related to the cylindrical Bessel functions of first and second kind, $J_\nu(z)$ and $Y_\nu(z)$, as follows (Abramowitz and Stegun 1972):

$$j_n(z)=\sqrt{\frac{\pi}{2z}}J_{n+\frac{1}{2}}(z),\quad y_n(z)=\sqrt{\frac{\pi}{2z}}Y_{n+\frac{1}{2}}(z). \tag{19}$$

The Green's function G needs to satisfy the boundary condition at infinity specified in (4). That is, it must exhibit the behavior of an outgoing wave. This is achieved if $R(r)$ satisfies the Sommerfeld radiation condition (Crighton *et al.* 1992)

$$\lim_{r\to\infty} r\left(\frac{\partial R}{\partial r}-\mathrm{i}kR\right)=0. \tag{20}$$

The solution (18) must then be expressed as

$$R(r)=\tilde{B}_1j_n(kr)+\tilde{B}_2h_n^{(1)}(kr), \tag{21}$$

where $h_n^{(1)}(z)$ is the spherical Hankel function, given by $h_n^{(1)}(z)=j_n(z)+\mathrm{i}y_n(z)$. This function satisfies (20) and thus has the appropriate outgoing wave behavior.

The complete solution to (17) is

$$\Theta(\theta)=C_1P_n(\cos\theta)+C_2Q_n(\cos\theta), \tag{22}$$

where P_n is the Legendre polynomial (i.e. the Legendre function of first kind) of degree n and Q_n is the Legendre function of the second kind, degree n (Abramowitz and Stegun 1972). It is noted that $Q_n(\cos\theta)\to\infty$ for $\cos\theta\to1$, i.e. for $\theta\to0$. The constant C_2 must then necessarily be 0.

It is recalled that P_n is equal to P_n^0, where P_n^m are the associated Legendre functions; these are related to P_n by:

$$P_n^m(z)=(-1)^m(1-z^2)^{\frac{m}{2}}\frac{d^mP_n(z)}{dz^m}. \tag{23}$$

It is to be noted that $P_n^m(z)\equiv0$ for $n<m$. For later use, it is also noted here that use of (23) gives

$$\frac{\partial P_n(\cos\theta)}{\partial\theta}=P_n^1(\cos\theta), \tag{24}$$

$$\frac{\partial^2P_n(\cos\theta)}{\partial\theta^2}=\cot\theta P_n^1(\cos\theta)+P_n^2(\cos\theta).$$

Next the delta function $\delta(\theta-\theta_*)/\sin\theta$ is expanded in a series in terms of $P_n(\cos\theta)$. The result is

$$\frac{\delta(\theta-\theta_*)}{\sin\theta} = \frac{1}{2}\sum_{n=0}^{\infty}(2n+1)P_n(\cos\theta_*)P_n(\cos\theta). \tag{25}$$

The Green's function $G(r,\theta)$ is expanded in the same way:

$$G(r,\theta) = \frac{1}{2}\sum_{n=0}^{\infty}(2n+1)P_n(\cos\theta_*)P_n(\cos\theta)G_n(r). \tag{26}$$

Inserting this expression into (14) gives again (16), but with $-\delta(r-r_*)/r^2$ as the right hand side. Using the standard solution technique (e.g. Sobolev (1989)), the solution (Green's function) for this problem takes the form

$$G_n(r) = \mathrm{i}k\begin{cases} j_n(kr)h_n^{(1)}(kr_*), & r<r_*, \\ j_n(kr_*)h_n^{(1)}(kr), & r>r_*. \end{cases} \tag{27}$$

Inserting (27) into (26) we finally obtain

$$G(r,\theta) = \frac{\mathrm{i}k}{2}\sum_{n=0}^{\infty}(2n+1)P_n(\cos\theta_*)P_n(\cos\theta)\begin{cases} j_n(kr)h_n^{(1)}(kr_*), & r<r_*, \\ j_n(kr_*)h_n^{(1)}(kr), & r>r_*. \end{cases} \tag{28}$$

4 Near- and far-field approximations

Taylor expansion in the near field

To facilitate a relatively simple evaluation of $\tilde{p}$, the sound pressure difference across the end plate, a Taylor expansion is used for both $j_n(z)$, and $h_n^{(1)}(z)$, assuming that the argument $z \ll 1$ ($z = kr$ or kr_*):

$$j_n(z) \approx b_{jn}z^n, \quad b_{jn} = \frac{1}{1\cdot 3\cdot 5\cdots(2n+1)} = \frac{\sqrt{\pi}}{2^{n+1}}\frac{1}{\Gamma(n+\frac{3}{2})}, \tag{29}$$

$$y_n(z) \approx b_{yn}z^{-(n+1)}, \quad b_{yn} = -1\cdot 3\cdot 5\cdots(2n-1) = -\Gamma(n+\tfrac{1}{2})\frac{2^n}{\sqrt{\pi}}, \tag{30}$$

where $\Gamma(n)$ is the gamma function (Abramowitz and Stegun 1972). Thus

$$h_n^{(1)}(z) \approx b_{jn}z^n + \mathrm{i}b_{yn}z^{-(n+1)}. \tag{31}$$

These expressions are used in (28). Application of the inverse Fourier transform (6) gives, for $r > r_*$, the time-domain 'near-field' Green's function

$$\begin{aligned} \mathcal{G}(r,\theta) \;=\; & \frac{1}{2}\sum_{n=0}^{\infty}(2n+1)P_n(\cos\theta)P_n(\cos\theta_*)\times \\ & \times\left\{(-1)^{n+1}\frac{b_{jn}^2}{c_0^{2n+1}}(rr_*)^2\delta^{(2n+1)}(t) - b_{jn}b_{yn}\frac{r_*}{r^2}\delta(t)\right\}, \quad \frac{r}{r_0}\ll 1, \end{aligned} \tag{32}$$

where $\delta^{(2n+1)}(t) = \partial^{2n+1}\delta(t)/\partial t^{2n+1}$. It is noted that (32) does not involve evaluation at a retarded time, due to the near-field assumption, i.e., the use of (29) and (30). For $r < r_*$, r and r_* should simply be interchanged in (32).

The derivatives of the delta function in (32) are to be interpreted in terms of the theory of generalized functions. That is, they are to be moved over to act on the 'ordinary' functions of the integrand in which they appear, via integration by parts.

Asymptotic expansion in the far field

For evaluating the sound pressure away from the end plate, an asymptotic expansion is used for $h_n(z)$, assuming that $z = kr \gg 1$:

$$h_n^{(1)}(z) \sim z^{-1} \mathrm{e}^{\mathrm{i}(z - n\frac{\pi}{2} - \frac{\pi}{2})}. \tag{33}$$

Using again that $z_* = kr_* \ll 1$, and thus that $r > r_*$, the Taylor expansion (29) is still applied for $j_n(z_*)$.

Employing the inverse Fourier transform (6), the time-domain 'far-field' Green's function can be evaluated as

$$\mathfrak{G}(r,\theta) = \frac{1}{2}\sum_{n=0}^{\infty}(2n+1)P_n(\cos\theta)P_n(\cos\theta_*)\frac{b_{jn}}{c_0^n}\frac{r_*^n}{r}\delta^{(n)}(t - r/c_0), \quad \frac{r}{r_0} \gg 1, \tag{34}$$

where $\delta^{(n)} = \partial^n\delta/\partial t^n$. It is noted that (34) involves evaluation at the retarded time $t - r/c_0$, on the contrary to (32); this enters via the exponential function of (33).

Applying again the inverse Fourier transform (6) to (12) gives, with use of (34), the far-field pressure as

$$\begin{aligned} p(r,\theta,t) \;=\; & \frac{\rho}{2}\sum_{i=1}^{I_{\mathrm{vtx}}}\sum_{n=0}^{\infty}(2n+1)\Bigg[P_n(\cos\theta)P_n(\cos\theta_i)\times \\ & \times\left\{\left[\frac{\partial^n}{\partial t^n}(u_{\theta_i}\Gamma_i)\right]_{t_r}\frac{r_i^{n-1}}{r}\frac{b_{jn}}{c_0^n} + \left[\frac{\partial^{n+2}}{\partial t^{n+2}}(u_{\theta_i}\Gamma_i)\right]_{t_r}\frac{r_i^{n+1}}{r}\frac{b_{jn+1}}{c_0^{n+2}}\right\} \\ & + P_n(\cos\theta)P_n^1(\cos\theta_i)\left[\frac{\partial^n}{\partial t^n}(u_{r_i}\Gamma_i)\right]_{t_r}\frac{r_i^{n-1}}{r}\frac{b_{jn}}{c_0^n}\Bigg] \\ & + \int_{r_\beta}\int_{\theta_\beta}\frac{1}{2}\sum_{n=0}^{\infty}(2n+1)\Bigg[P_n(\cos\theta)P_n(\cos\theta_\beta)\times \\ & \times\left\{\left[\frac{\partial^n\tilde{p}}{\partial t^n}\right]_{t_r}\frac{r_\beta^{n-1}}{r}\frac{b_{jn}}{c_0^n} + \left[\frac{\partial^{n+2}\tilde{p}}{\partial t^{n+2}}\right]_{t_r}\frac{r_\beta^{n+1}}{r}\frac{b_{jn+1}}{c_0^{n+2}}\right\}n_{r_\beta} \\ & + P_n(\cos\theta)P_n^1(\cos\theta_\beta)\left[\frac{\partial^n\tilde{p}}{\partial t^n}\right]_{t_r}\frac{r_\beta^{n-1}}{r}\frac{b_{jn}}{c_0^n}n_{\theta_s}\Bigg]r_\beta^2\sin\theta_\beta dr_\beta d\theta_\beta, \end{aligned} \tag{35}$$

which is valid for $r/r_0 \gg 1$. In (35) the vortex ring coordinates r_i, θ_i play the role of the source coordinates r_*, θ_*. Square brackets with subscript t_r indicate evaluation at the retarded time t_r. It is to be remarked that (35) is valid only when the observation point radius $r > r_i$. [The case $r < r_i$ is not of interest here.] Evaluation of the pressure difference $\tilde{p}$ is discussed in the next section.

Equation (35) is a multipole expansion of the sound field. A term of order of magnitude $c_0^{-n}\partial^n/\partial t^n$ correspond to a pole of order 2^n (Howe 1998). Thus, terms proportional to $\mathfrak{L} = \boldsymbol{\omega}\times\mathbf{u}$ and $\tilde{p}$ correspond to monopoles; terms proportional to $\partial\mathfrak{L}/\partial t$ and $\partial\tilde{p}/\partial t$ correspond to dipoles; and terms proportional to $\partial^2\mathfrak{L}/\partial t^2$ and $\partial^2\tilde{p}/\partial t^2$ correspond to quadrupoles.

5 Numerical implementation

Discretization of the boundary integrals

The boundary integrals appearing in (35) and in the time-domain version of (12) are evaluated numerically by employing the boundary element method (BEM). The end plate, which is the

only acoustically significant boundary in the present problem, is discretized into N_e elements. The pressure difference across each element is represented by

$$p_e(r_\beta, \theta_\beta) = \sum_{n=1}^{N_{\rm nod}} \psi_n(r_\beta, \theta_\beta)\tilde{p}_{en}, \tag{36}$$

where $\psi_n(r_\beta, \theta_\beta)$ are interpolation functions, and $N_{\rm nod}$ the number of nodes within each element. Inserting (36) into (13) gives, with application of (6),

$$\sum_{e=1}^{N_e}\sum_{n=1}^{N_{\rm nod}} \int_{-\infty}^{\infty} \tilde{P}_{en} \iint \psi_n \frac{\partial^2 G(r_\alpha, \theta_\alpha; r_{\beta e}, \theta_{\beta e})}{\partial n_\alpha \partial n_{\beta e}} r_{\beta e}^2 \sin\theta_{\beta e} dr_{\beta e} d\theta_{\beta e} \mathrm{e}^{-\mathrm{i}\nu t} d\nu$$
$$= \rho \sum_{i=1}^{I_{\rm vtx}} \int_{-\infty}^{\infty} \frac{\partial^2 G(r_\alpha, \theta_\alpha; r_i, \theta_i)}{\partial n_\alpha \partial (r_i, \theta_i)} \mathfrak{L}_i(r_i, \theta_i, \nu)\, \mathrm{e}^{-\mathrm{i}\nu t} d\nu, \tag{37}$$
$$\alpha = 1, 2, \ldots, N_e,$$

where $\partial^2 G/\partial n_\alpha \partial(r_i, \theta_i)$ stands for $\partial^2 G/\partial n_\alpha \partial r_i + \partial^2 G/\partial n_\alpha \partial \theta_i$.

Time integration of the plate pressure difference $\tilde{p}$

Evaluation of (37) at the Ne elements gives an equation system on the form

$$\mathbf{A}_0\tilde{\mathbf{p}} + \mathbf{A}_2 \frac{1}{c_0^2}\frac{\partial^2 \tilde{\mathbf{p}}}{\partial t^2} + \cdots = \mathbf{b}_0(\mathfrak{L}) + \mathbf{b}_2(c_0^{-2}\partial^2 \mathfrak{L}/\partial t^2) + \cdots . \tag{38}$$

(No terms proportional to $c_0^{-1}\partial\tilde{p}/\partial t$ and $c_0^{-1}\partial\mathfrak{L}/\partial t$ are present.)

Equation (38) is solved in a time-stepping fashion, including up to second derivatives. At step n, say, the system is then solved with respect to $\partial^2\tilde{\mathbf{p}}_{n+1}/\partial t^2$, with the first term on the left hand side moved to the right hand side, as follows:

$$\mathbf{A}_2 \frac{1}{c_0^2}\frac{\partial^2 \tilde{\mathbf{p}}_{n+1}}{\partial t^2} = \mathbf{b}(\mathfrak{L}, \partial^2\mathfrak{L}/\partial t^2, \ldots) - \mathbf{A}_0\tilde{\mathbf{p}}_n. \tag{39}$$

The pressure and its first derivative are updated using the trapezoidal rule:

$$\begin{aligned} \frac{\partial \tilde{\mathbf{p}}_{n+1}}{\partial t} &= \frac{\partial \tilde{\mathbf{p}}_n}{\partial t} + \frac{\Delta t}{2}\frac{\partial^2 \tilde{\mathbf{p}}_n}{\partial t^2} + \frac{\partial^2 \tilde{\mathbf{p}}_{n+1}}{\partial t^2}, \\ \mathbf{p}_{n+1} &= \mathbf{p}_n + \frac{\Delta t}{2}\left(\frac{\partial \mathbf{p}_n}{\partial t} + \frac{\partial \mathbf{p}_{n+1}}{\partial t}\right). \end{aligned} \tag{40}$$

Equations (39) and (40) constitute a method which is stable for any value of the time step Δt.

6 Computational details and a numerical example

A numerical example will be given for geometric and physical data corresponding to the experimental setup of Nakano *et al.* (2004) with nozzle and end plate hole diameter $d_0 = 2r_0$ equal to 50 mm. The experimental end plate is rectangular, with dimensions 200 mm (height) × 270 mm (width). But in the numeric model it is necessary to consider an axisymmetric (circular) end plate. The outer diameter d_1 is taken to be 250 mm; that is, $d_1 = 5d_0$. The gap length ℓ is 50 mm, e.g., equal to d_0. The mean velocity u_0 of the air-jet is 10 m/s. [This velocity gives the 'sharpest' sound in the experiments.] At 20 °C this corresponds to a Reynolds number $Re = u_0\, d_0/\hat{\nu} \approx 3.3 \times 10^4$ and a Mach number $M = u_0/c_0 \approx 0.03$, where the speed of sound c_0 = 340 m/s and the kinematic viscosity $\hat{\nu} = 1.5 \times 10^{-5}$ m^2/s.

Based on the studies in Langthjem and Nakano (2005) the time-step was chosen as $\Delta t = 0.025 d_0/u_0$. Simulations were carried out in 3200 time-steps, in order to obtain transient-free time series. The frequency spectrum (see below) was obtained by analyzing the last $2^{11} = 2048$ of these 3200 data sets via fast Fourier transform (Press *et al.* 1992). The first 1152 data sets were discarded, as transients. With the time-step Δt as given above, and with $N = 2048$ steps, the resolution of the frequency spectrum is $\Delta f = 1/N\Delta t = 40u_0/Nd_0 \approx 4\,\mathrm{Hz}$. The Nyquist critical frequency is $f_c = 1/2\Delta t = 4\,\mathrm{kHz}$.

The end plate was discretized into 24 uniformly distributed panels. The simplest possible elements, with one node per element ($N_{\mathrm{nod}} = 1$), were applied. The interpolation function ψ_1 in (36) is then simply equal to 1, which implies constant pressure within each element.

The differentiation of the velocities in (35) must necessarily be evaluated numerically. A simple finite difference approach will typically produce too much numerical 'jitter', especially for the second derivatives. To avoid this the differentiation was carried out using a Savitsky-Golay smoothing filter (Press *et al.* 1992). A so-called casual filter was applied, which fits a polynomial to the pressure at the actual time step and a number of earlier pressure data points. The polynomial is then differentiated. This approach effectively eliminates excessive 'numerical noise'. A fourth order polynomial was fitted to 16 data points. Other values of both polynomial order and number of data points were also tried. The results are not very sensitive to changes in these values.

Experimental and computational sound pressure spectra for the observation point $(x, r) = (0.5, 1.84)d_0$ (in terms of cylindrical coordinates) are compared in Figure 3. [In spherical coordinates the observation point is at $(r, \theta) = (1.907d_0, 74.80°)$. It is remarked that this location basically violates the far field assumption $r/r_0 \gg 1$. It was chosen in the experiments (Nakano *et al.* 2004) in order to avoid disturbing reflections from walls and things in the room.] The locations of the main frequency component f_0 and its higher harmonics, $2f_0, 4f_0, \ldots$, agree well; the peak values also agree reasonably well. The broadband noise level is however higher in the computations than in the experiments. This is likely due to the neglect of viscous effects.

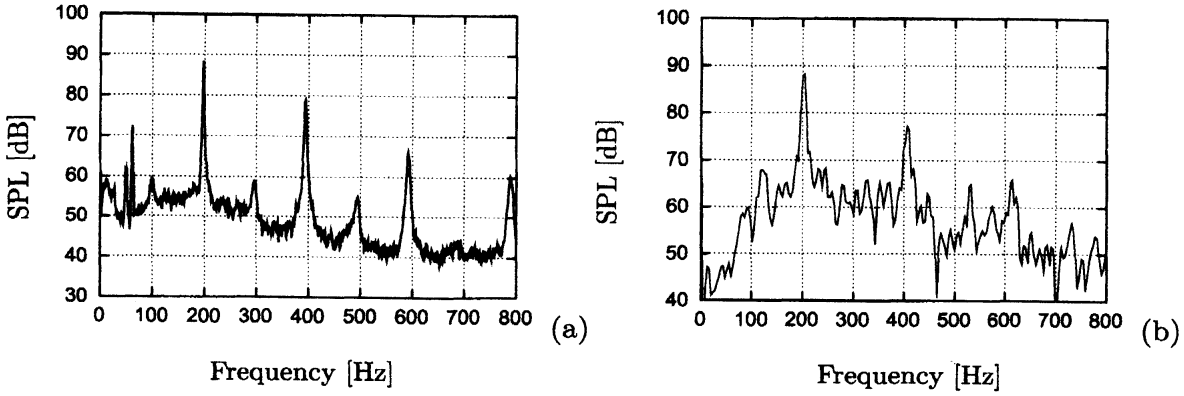

Figure 3: Frequency spectrum of the acoustic pressure at the position $(x, r) = (0.5, 1.84)d_0$ (in cylindrical polar coordinates). (a) Experimental. (b) Numerical.

Acknowledgement

The support of the present project through a JSPS Grant-in-Aid for Scientific Research (No. 18560152) is gratefully acknowledged.

References

Abramowitz, M., Stegun, I.A., 1972. *Handbook of Mathematical Functions*, Dover Publications, New York.

Chanaud, R.C., Powell, A., 1965. Some experiments concerning the hole and ring tone, *J. Acoust. Soc. Am.* 37, 902-911.

Crighton, D. G., Dowling, A. P., Ffowcs Williams, J. E., Heckl, M., Leppington, F. G., 1992. *Modern Methods in Analytical Acoustics*, Springer Verlag, London.

Howe, M. S., 1975. Contributions to the theory of aerodynamic sound, with applications to excess jet noise and the theory of the flute, *J. Fluid Mech.* 71, 625-673.

Howe, M. S., 1998. *Acoustics of Fluid-Structure Interaction*, Cambridge University Press, Cambridge UK.

Howe, M. S., 2003. *Theory of Vortex Sound*, Cambridge University Press, Cambridge UK.

Lamb, H., 1993. *Hydrodynamics*, Cambridge University Press, Cambridge UK, (Originally published in 1932).

Langthjem, M.A., Nakano, M., 2005. A numerical simulation of the hole-tone feedback cycle based on an axisymmetric discrete vortex method and Curle's equation, *Journal of Sound and Vibration* 288, 133-176.

Nakano, M., Tsuchidoi, D., Kohiyama, K., Rinoshika, A., Shirono, K., 2004. Wavelet analysis on behavior of hole-tone self-sustained oscillation of impinging circular air jet subjected to acoustic excitation, *Kashikajouhou* 24, 87-90 [In Japanese].

Nitsche, M., Krasny, R., 1994. A numerical study of vortex ring formation at the edge of a circular tube, *Journal of Fluid Mechanics*, 276, 139-161.

Petrovsky, I.G., 1991. *Lectures on Partial Differential Equations*, Dover Publications, New York.

Powell, A., 1964. Theory of vortex sound. *J. Acoust. Soc. Am.* 36, 177-195.

Press, W.H., Teukolsky, S.A., Vetterling, W.T., Flannery, B.P., 1992. *Numerical Recipes in FORTRAN. The Art of Scientific Computing* (2nd ed), Cambridge University Press, Cambridge.

Lord Rayleigh, 1945. *The Theory of Sound*, Vol. II, Dover Publications, New York.

Rockwell, D., Naudascher, E., 1979. Self-sustained oscillations of impinging free shear layers. *Annu. Rev. Fluid Mech.* 11, 67-94.

Rockwell, D., 1983. Oscillations of impinging shear layers. *AIAA J.* 21, 645-664.

Sobolev, S.L., 1989. *Partial Differential Equations of Mathematical Physics*, Dover Publications, New York.

Terai, T., 1980. On calculation of sound fields around three dimensional objects by integral equation methods, *Journal of Sound and Vibration* 37, 71-100.